STScI | SPACE TELESCOPE SCIENCE INSTITUTE

Instrument Science Report ACS 2017-13

Accounting for Readout Dark in ACS/WFC Superbiases

J. E. Ryon, N. A. Grogin, D. Coe

December 22, 2017

Abstract

We investigate the properties of excess dark current accumulated during the 100-second full-frame readout of the Advanced Camera for Surveys (ACS) Wide Field Channel (WFC) detectors. This excess dark current, called "readout dark", gives rise to ambient background gradients and hot columns in each ACS/WFC image. We present an analysis of simulated readout dark images developed in ACS ISR 2014-02, and find that the results from the simulated data cannot be fully reconciled with the results from observed bias images. We develop a new method to estimate the readout dark noise properties in ACS/WFC observations instead of using simulated images. While readout dark signal is removed from science images during the bias correction step in CALACS, the additional noise from the readout dark is currently not taken into account. We will update the ERR extensions of superbias images to include the appropriate noise from the ambient readout dark gradient and stable hot columns. We will also flag unstable hot columns in the DQ extensions of the superbiases. A new reference file pipeline for ACS/WFC that will implement these changes is currently under construction.

1 Introduction

The Advanced Camera for Surveys (ACS) was installed on the Hubble Space Telescope (HST) in March 2002. Since then, radiation damage has given rise to a number of defects in the Wide Field Channel (WFC) detectors, including an ever-increasing number of hot pixels

and average dark current. As each ACS/WFC image is read out, dark current continues to accumulate in the pixels, resulting in excess "readout dark". At the same time, extremely hot pixels leak dark electrons, producing hot columns.

Because readout dark is present in every frame observed with ACS/WFC, it is difficult to characterize. Bias frames are the most useful type of image for studying the effects of readout dark because only bias structure and readout dark are present. The twenty to thirty biases taken between CCD anneals are combined into a "superbias" with ACSREJ (Lim et al., 2012). ACSREJ computes the ERR extension of the output image by summing the ERR extensions of the input images in quadrature, excluding the contribution from pixels in each frame that are affected by cosmic rays. The ERR extensions of a bias contain the readnoise of each amplifier, so the superbias ERR extension is simply the readnoise divided by the square root of the number of biases in the anneal cycle[1] (Lucas & et al., 2016). The superbias DQ extensions contain bias structure flags for pixels that exceed a somewhat arbitrarily established threshold value of 8 electrons in the smoothed SCI extensions (Lim et al., 2012).

Fortunately, removing readout dark signal and bias structure from science frames is simple: perform BIASCORR within CALACS to subtract the superbias from the SCI extensions of the science frames. The additional noise from readout dark, however, is not currently included in the ERR extensions of the superbiases, which means it is not propagated to the science frames processed by the superbiases. In particular, if the hot columns that arise during the readout process are stable over an anneal period, then they will be properly subtracted during BIASCORR. The additional noise from these stable hot columns should be included in the ERR extension and the hot columns themselves should not be flagged in the DQ extension. Unstable hot columns cannot be properly subtracted from science images. Therefore, they should be flagged as bias structure, flag 128, in the superbias DQ extensions, which will allow users to remove these pixels from their analysis. The new treatment of hot columns in superbiases described in this report is intended to reflect the stability analysis of hot pixels in superdarks as described in Borncamp et al. (2017).

An earlier study of readout dark in ACS/WFC images was presented in Coe & Grogin (2014) (CG14), which showed that readout dark in each quadrant increases with distance from the amplifier. CG14 also quantified the additional signal and noise present in ACS/WFC images due to readout dark and developed a method for simulating readout dark images using superdark images. While CG14 also showed that the simulated images reproduce the observed noise in bias images fairly well, further investigation and implementation are required.

The purpose of this study is to continue the work by CG14 to fully characterize the readout dark and account for it in each superbias from the lifetime of ACS. In Section 2, we further test the efficacy of simulated readout dark images from CG14, including almost four years of new data, and find that we prefer to measure the effects of readout dark directly from bias images. In Section 3, we describe the steps taken to update the superbias ERR and DQ extensions. In Section 4, we summarize this work.

[1]Pixels hit by cosmic rays will have slightly higher ERR values because the number of biases contributing to these pixels has been reduced.

2 Testing Simulated Readout Darks

We revisit the investigation of simulated readout dark images developed by CG14, including four additional years of data. In particular, we focus on comparing the readout dark predicted by the simulated images and that measured in observed biases over the lifetime of ACS/WFC. If the simulated readout dark images match the observed expectations, we will update the ACS/WFC reference file pipeline to combine the simulated data with the ERR extensions of the superbiases. If the opposite is true, we will develop a new method to estimate the readout dark contribution from observed biases. Additional analysis of hot column stability is required in either case.

A description of the simulated images can be found in Section 4 of CG14, and we also provide relevant details here. The amount of readout dark signal deposited in a given row is determined by the delay between the end of the exposure and the time at which the row is read out. To simulate this process, each row in a superdark image is summed with the rows nearer to the amplifier, resulting in an array containing the cumulative dark current each pixel encounters (in e−/sec). Each row is multiplied by the readout time for a single row, about 49 milliseconds. The result is an estimate of the dark electrons accumulated in each pixel during the readout process, or the "pure" readout dark. Each pixel is resampled from a Poisson distribution defined by its value in the "pure" readout dark, which assumes that the dark current deposition is Poissonian in nature. The appropriate readnoise for each quadrant is included to produce a final readout dark image. The final image is similar to a bias frame, though it does not include the 2D bias gradient or bias striping, which arose after the electronics were replaced during Servicing Mission 4 (SM4) (Golimowski et al., 2011). Other features like cosmic rays and CTE losses are also not reproduced by the simulated images. See Figure 11 in CG14 for examples of these simulated images.

2.1 Ambient Readout Dark Effects

To test the simulated readout dark images, we first measure the increase in signal in "normal" (not hot or warm) pixels due to readout dark, which we will call "ambient" readout dark signal. It appears as a gradient along the rows in each quadrant of the detector because the amount of signal deposited increases with distance from the amplifier.

Procedure I: Measuring Readout Dark Signal from Simulated Data

1. Produce simulated readout dark images using about 70 superdarks covering the lifetime of ACS.

2. Identify and remove hot columns:

   (a) Average the columns of the 20 rows furthest from the amplifier.

   (b) Ignore columns >3×NMAD[2] from the median average column value.

3. Measure signal increase across the detector:

[2]Normalized Median Absolute Deviation, a measure of the standard deviation of a distribution that is more robust to outliers: $\mathrm{NMAD}(x) = 1.4826 \times \mathrm{median}\left(|x - \mathrm{median}(x)|\right)$.

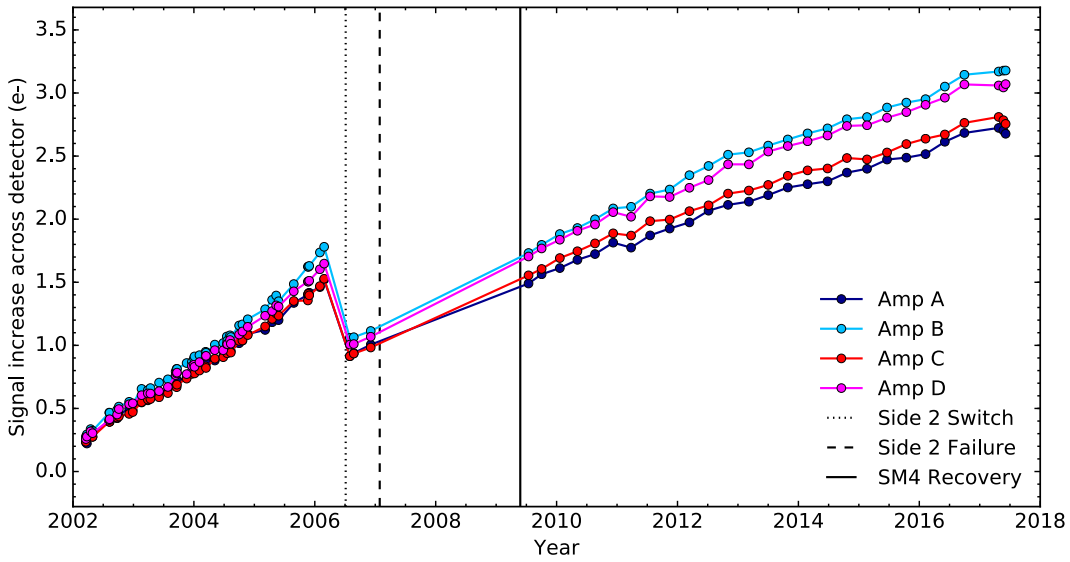

Figure 1: Simulated ambient signal increase across the detector due to readout dark, in e−, over the lifetime of ACS. The signal increase was measured from simulated readout dark images as described in Procedure I. Each quadrant is labeled by the amplifier designation. The dates of the switch to side 2 electronics, the failure of side 2 electronics, and the SM4 recovery of ACS/WFC are also indicated by dotted, dashed, and solid black lines, respectively.

(a) Average the rows of the remaining columns.

(b) Perform a linear fit to the average column as a function of row number.

(c) Subtract the endpoints of the fit, $\Delta S = b_{y=2048} - b_{y=0}$, where ΔS is the signal increase due to readout dark, and the b values are the y-intercepts of the linear fit at row 2048 and row 0 in the orientation of amp C.

In Figure 1, we plot the ambient signal increase over the lifetime of ACS. The ambient signal increase has grown at a nearly constant rate in all four quadrants since late 2009, after the SM4 recovery. The ambient signal increase between ACS installation (2002) and the temperature decrease associated with the switch to side 2 electronics (2006) grew more rapidly. In addition, it appears that the rate of increase has been slightly larger for Amps B and D than Amps A and C post-SM4.

Next, we measure the observed ambient readout dark signal in raw bias images taken during each anneal cycle from the lifetime of ACS. The method is similar to that for the simulated data, with a few differences necessary to isolate readout dark in observed data (highlighted in bold in the steps below). This method also largely matches that described in Section 2 of CG14.

Procedure II: Measuring Readout Dark Signal from Observed Data

1. **Ignore the first four biases from the anneal cycle to allow for settling of the command voltages.**

2. Identify and remove hot columns and **cosmic rays from each bias**:
   (a) Average the columns of the 20 rows of the **virtual overscan**.
   (b) Ignore columns >3×NMAD from the median average column value.
   (c) **Sigma-clip along the columns in each quadrant, rejecting 3-sigma outliers and iterating five times.**
3. **Remove bias structure from the science columns, leaving only readout dark:**
   (a) **Average the rows of the last four columns of the physical prescan (columns 21-24 in the orientation of amp C)**[3].
   (b) **Subtract average prescan column from the fifty science columns nearest to the prescan (columns 25-74).**
4. Measure signal increase across the detector:
   (a) Average the rows of the remaining columns.
   (b) **Average together the average columns from all of the bias images in the anneal cycle.**
   (c) Perform a linear fit to the final average column as a function of row number.
   (d) Subtract the endpoints of the fit, $\Delta S = b_{y=2048} - b_{y=0}$, where ΔS is the signal increase due to readout dark, and the b values are the y-intercepts of the linear fit at row 2048 and row 0 in the orientation of amp C.

In Figure 2, we plot the observed ambient signal increase in raw bias images from anneal cycles over the lifetime of ACS. Similar to the simulated signal increase in Figure 1, the observed signal increase shows a clear positive trend for all four quadrants since late 2009. There is also a positive trend prior to the switch to side 2 electronics in 2006, and the magnitude of the observed signal increase matches fairly well with the simulated data in that time period. However, post-SM4, the observed signal increase ranges from 30 to 150% larger than simulated, depending on quadrant and date. Also, the quadrants with the largest observed signal increase appear to be Amps A and C, which is opposite to the simulated data. These results agree with Figure 5 in CG14, though the authors used the last four science columns instead of the first fifty to measure the readout dark signal increase.

We next measure the ambient *variance* increase across the detector due to readout dark alone in both simulated and observed data. In fact, the variance increase due to readout dark is more relevant for our analysis than the signal increase because it is one of the components we will include in the ERR extensions of the superbiases. Also, despite our attempts to mitigate the effects of the 2D bias gradient in the observed signal increase measurement (Step 2 of Procedure II), the prescan column may not remove all of the bias gradient from the science columns, and therefore it may contaminate the signal increase results. For the *variance* increase, however, we ensure that fixed bias structure like the bias gradient is removed by performing our analysis on differenced consecutive biases.

[3]This average prescan column should provide a good estimate of the bias level, bias striping, and vertical component of the 2D bias gradient, particularly for columns close to the prescan (Golimowski et al., 2011).

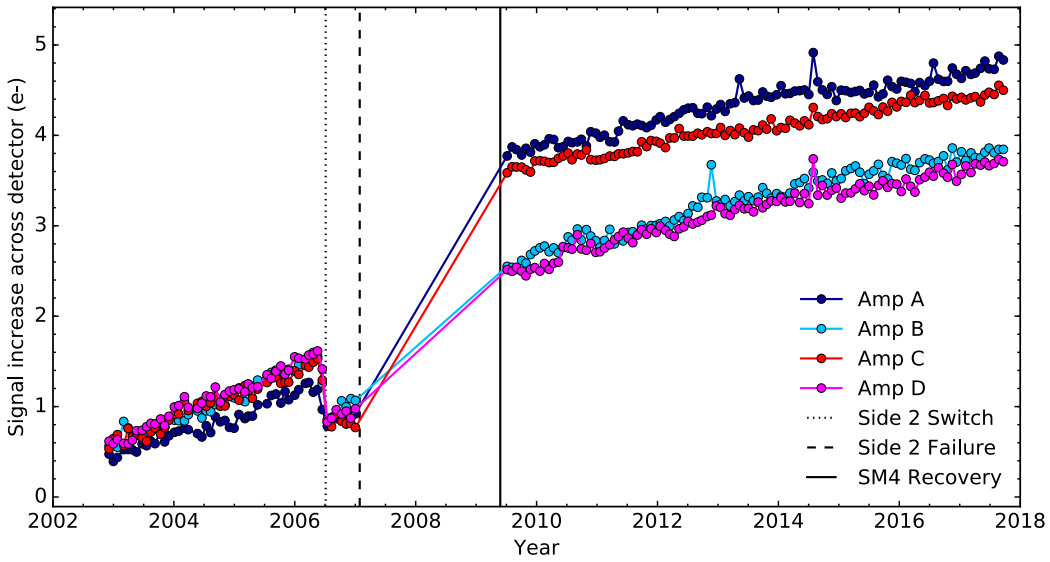

Figure 2: Same as Figure 1, but for observed ambient signal increase across the detector due to readout dark, in e−, over the lifetime of ACS. The signal increase was measured from raw bias images as described in the text.

Procedure III: Measuring Readout Dark Variance from Simulated Data

Only Step 3 from Procedure I changes when measuring the variance increase, Steps 1 and 2 remain the same.

3. Measure variance increase across the detector:
   (a) Measure the ambient noise in each row by taking the standard deviation.
   (b) Perform a linear fit to the noise values as a function of row number.
   (c) Subtract the squares of the endpoints of the fit, $\Delta\sigma^2 = b^2_{y=2-048} - b^2_{y=0}$, where $\Delta\sigma^2$ is the variance increase due to readout dark, and the b values are the y-intercepts of the linear fit at row 2048 and row 0 in the orientation of amp C.

In Figure 3, we plot the ambient variance increase in simulated readout dark images using about 70 superdarks taken over the lifetime of ACS. The evolution of the simulated ambient variance increase appears nearly identical to that of the simulated ambient signal increase in Figure 1, but the variance is typically about 25% larger than the signal.

Next, we measure the observed ambient readout dark variance in raw bias images taken during each anneal cycle from the lifetime of ACS. The method is similar to that for the simulated data, with a few differences necessary to isolate readout dark in observed data (highlighted in bold in the steps below).

Procedure IV: Measuring Readout Dark Variance from Observed Data

1. **Remove fixed bias structure, like bias gradient:**

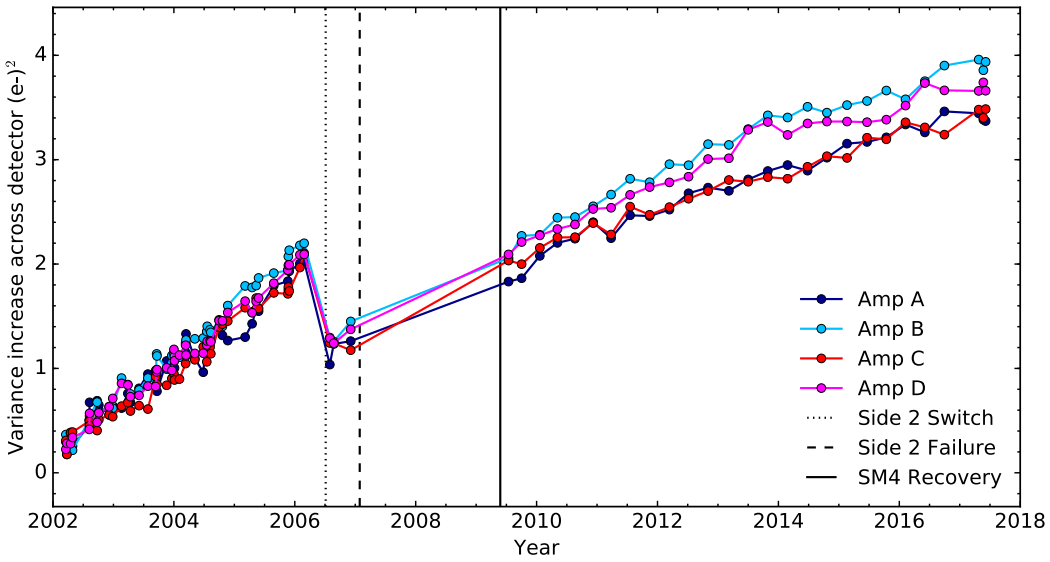

Figure 3: Same as Figure 1, but for simulated variance increase across the detector, in electrons squared, $(e-)^2$, due to readout dark as measured from simulated readout dark images over the lifetime of ACS.

(a) **Difference two consecutive biases. The noise of the resulting difference frame is increased by $\sqrt{2}$.**

Step 2 for removing hot columns and cosmic rays is the same as in Procedure II.

3. Measure variance increase across the detector:

   (a) Measure the ambient noise in each row by taking the standard deviation.

   (b) Perform a linear fit to the noise values as a function of row number.

   (c) Subtract the squares of the endpoints of the fit **and divide by two to remove the increased noise from Step 1,** $\Delta\sigma^2 = (b^2_{y=2-048} - b^2_{y=0})/2$, where $\Delta\sigma^2$ is the variance increase due to readout dark, and the b values are the y-intercepts of the linear fit at row 2048 and row 0 in the orientation of amp C.

   (d) **Average the variance increase measurements from all of the biases in the anneal cycle.**

In Figure 4, we plot the observed ambient variance increase in differences of raw bias images from about 30 anneal cycles over the lifetime of ACS. The evolution of the observed ambient variance increase appears nearly identical to that of the observed ambient *signal* increase in Figure 2, and the magnitudes are similar, within about 20% of each other. However, the magnitude of the observed variance is generally about 25 to 85% larger than simulated, particularly post-SM4.

Therefore, we find differences between the statistics of the simulated readout dark images and observed readout dark effects. In the measurement of ambient signal increase, the difference may be due to poor subtraction of the bias gradient from the science columns.

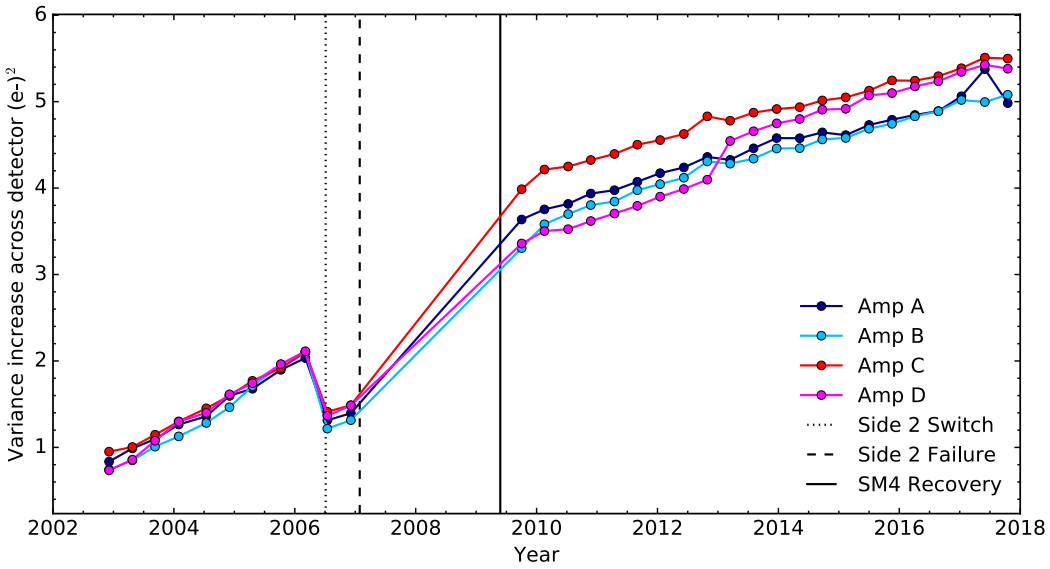

Figure 4: Same as Figure 1, but for observed variance increase across the detector in $(e-)^2$, due to readout dark as measured from raw biases over the lifetime of ACS.

However, we do expect the bias gradient to be completely removed when subtracting consecutive raw biases in the observed variance measurement. It therefore appears that the simulated readout dark images are not accounting for a significant fraction of the ambient readout dark variance. Our results agree overall with the analysis in CG14. However, we take the extra step of closely inspecting the readout dark variance alone, and the differences we find between the simulated and observed variance are too large to ignore. Possible explanations for this difference are that the superdarks used to model the readout dark may be underestimating the true ambient dark current, or that the readout dark model may be too simple to account for all of the additional noise from the readout process.

2.2 Hot Columns in Simulated Readout Darks

Hot columns arise when charge packets gain excess electrons from a hot pixel as they are transferred between rows to the readout register. Therefore, the pixels upstream of a hot pixel (in the opposite direction to the readout direction) may contain several excess electrons of readout dark signal. Because the noise in hot columns is greater than the average normal pixel, we must ensure that it is accurately included in the superbias ERR arrays.

We compare the hot columns present in the simulated readout dark images to those present in raw bias images to determine if the readout dark noise is properly represented. We perform our analysis in this section on images from a recent anneal cycle, 2015-07-01, as a test case, though we find similar results when running this analysis on data from other anneal cycles. The hot columns we analyze are selected from the superbias image for this anneal as described in Sections 3.2 & 3.3.

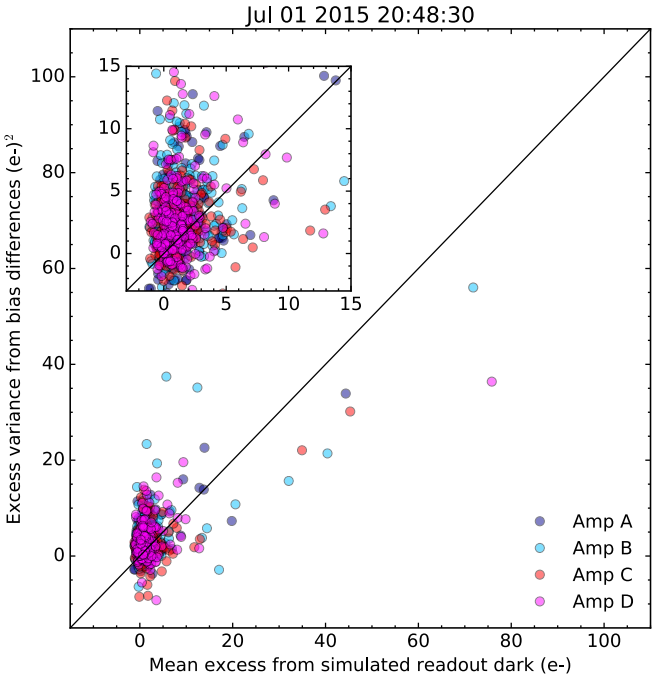

Figure 5: Excess variance from bias differences as a function of mean excess signal from the simulated readout dark for stable, hot columns found in the superbias from the 2015-07-01 anneal cycle. Hot columns in each quadrant are color-coded. If the readout dark current is Poisson-like, and the simulated readout dark is accurately modeling the hot columns, the points should lie along the black line. The inset plot shows a zoomed-in version of the location where the majority of the points lie.

Procedure V: Measuring Mean Excess in Hot Columns from Simulated Data

1. Generate simulated readout dark image using a superdark (in this case, *19p1349gj_dkc.fits*).
2. Calculate mean excess in each hot column:
   (a) Remove local background column from hot column in simulated image:
      i. Take median along the rows of eight neighboring columns and subtract result from the hot column[4].
   (b) Calculate the mean of the resulting "excess" column.

We compare the mean excess from simulated data to the excess *variance* in the same columns in bias difference images. If the deposition of readout dark electrons in the hot column is Poisson-like, then we would expect the excess variance from readout dark to be essentially equal to the mean excess in the simulated hot column[5].

[4]We take the local background from eight neighboring columns simply to mitigate the effect of nearby hot pixels and columns.

[5]This is because $N = \sqrt{S}$, where N is noise and S is signal for a Poisson process.

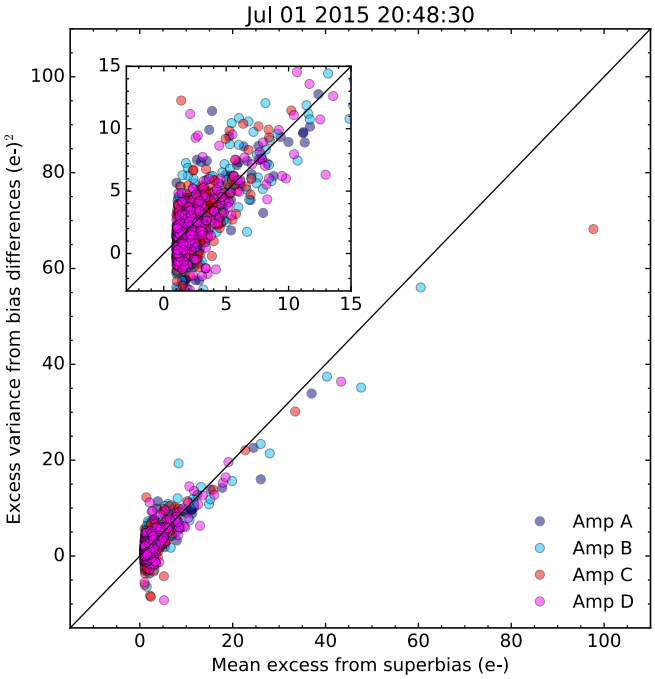

Figure 6: Same as Figure 5, but for mean excess values from the superbias for stable, hot columns from the 2015-07-01 anneal cycle.

Procedure VI: Measuring Excess Variance in Hot Columns from Observed Data

1. Remove fixed bias structure, like bias gradient:
   (a) Difference two consecutive biases. The noise of the resulting difference frame is increased by $\sqrt{2}$.
2. Identify and remove cosmic rays from each bias:
   (a) Sigma-clip along the hot column and eight neighboring columns, rejecting 3-sigma outliers and iterating five times.
3. Calculate excess variance in each hot column:
   (a) Calculate variance of the distribution of hot column pixel values and the variance of the neighboring columns over the anneal cycle.
   (b) Subtract the variance of the neighboring columns from that of the hot column.

In Figure 5, we plot the mean excess values from the simulated readout dark image and the excess variance values from the bias differences for each hot column. We would expect the points to cluster about the one-to-one relation (black line) if the simulated readout dark image were properly reproducing the hot columns. While some of the points cluster near zero, the majority of the columns lie significantly off the relation. Therefore, the readout dark

variance measured in the hottest (noisiest) columns in biases does not match the readout dark *signal* in the simulated images.

Next, we measure the hot column mean excess in the 2015-07-01 superbias using the same procedure as for the simulated readout dark images. We plot the mean excess values from the superbias and the excess variance values from the bias differences for each hot column in Figure 6. These values agree much more closely than those in Figure 5, indicating that the superbias hot columns appropriately reproduce the readout dark variance. We note that several of the hottest columns appear to exhibit less variance in the bias differences than expected from the superbias excesses, but this only occurs at very high mean excess values.

3 Updating Superbiases

Given the results presented in Section 2, we choose to estimate the contribution of readout dark to the noise properties of ACS/WFC observations directly from raw biases and superbiases instead of using the simulated readout dark images from CG14. We run several steps of analysis on the superbias itself and the set of raw biases listed in the HISTORY keyword of the superbias header:

1. Determine the increase in variance across each ACS/WFC detector chip due to ambient readout dark noise.

2. Identify hot columns in the superbias and calculate the mean excess signal in each hot column.

3. Determine the stability of each hot column over the time period spanned by the set of raw biases.

4. Combine the mean excesses of the stable hot columns with the ambient variance increase across each detector and the existing ERR extension of the superbias to produce a new ERR extension for the superbias.

5. Flag the unstable hot columns with the bias structure flag, 128, and unflag all others in the DQ extension of the superbias.

3.1 Ambient Variance Ramp

We calculate the increase in variance across each quadrant of the ACS/WFC detectors due to ambient readout dark noise with the same procedure as in Section 2.1. We generate an array for each quadrant that contains a linearly increasing ramp of variance, in units of electrons squared, $(\mathrm{e}-)^2$, from zero at the row nearest the amplifier to the total variance increase at the row furthest from the amplifier. We then concatenate these arrays into the proper orientation for the ACS/WFC detector and add rows and columns of zeros to represent the physical prescan and virtual overscan for each chip. As shown in Figure 4, the ambient variance increase in recent anneal cycles is $\sim$5.0 to 5.5 $(\mathrm{e}-)^2$.

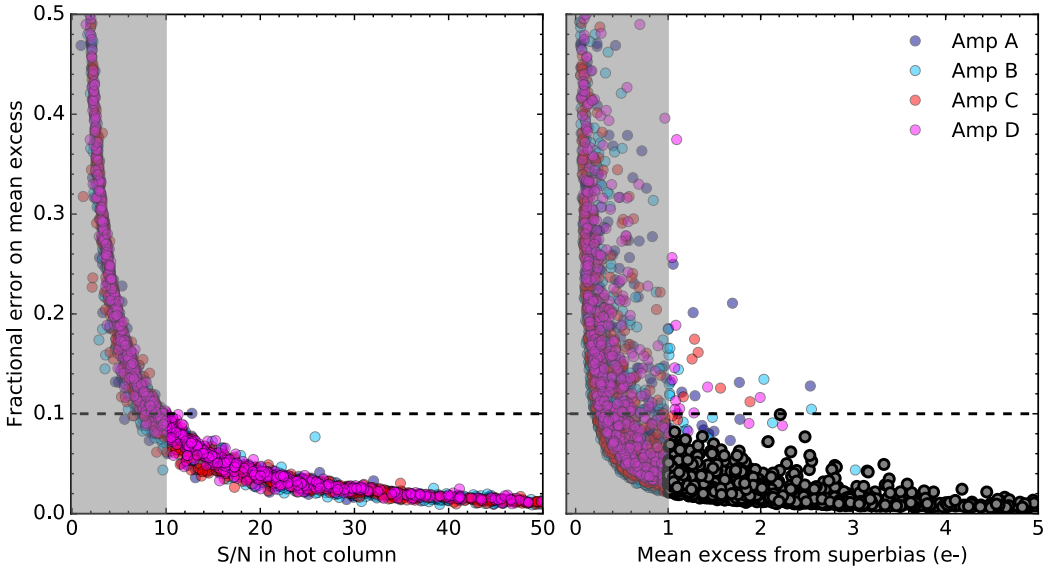

Figure 7: Fractional error of the mean excess in the hot columns as a function of S/N mean excess as measured in the superbias. Hot columns in each quadrant are color-coded. The gray shaded area covers rejected columns below the mean excess and S/N thresholds of 1 e− and 10, respectively. The dashed line represents a fractional error of 0.1 (10%). The gray points in the right panel are hot columns that satisfy both the mean excess and S/N thresholds.

3.2 Identify Hot Columns

We identify hot columns by considering every column in each quadrant of the superbias. We find the excess signal in each column by subtracting off the median along each row of eight neighboring columns. This should remove the local bias level and gradient, leaving only readout dark signal. Each column of excess values is then convolved with an edge detection kernel consisting of sixteen values of 1.0 followed by sixteen values of −1.0. The maximum of the resulting convolved column corresponds to the location of the largest change in a local average along the column, which, if a hot section exists, reliably matches the y-coordinate at which that section originates. We can then determine the mean excess signal and signal-to-noise ratio of the section. The S/N is defined as

$$S/N = \frac{\langle a \rangle \, L}{\sqrt{\langle a \rangle \, L + 9/8 \frac{(\mathrm{RN}^2 L + \mathrm{B}^2 L + \sigma^2_{\mathrm{amb}})}{n}}}, \tag{1}$$

where $\langle a \rangle$ is the mean of the excess signal in the column section, L is the length of the column section, RN is the readnoise for the quadrant, B is the bias striping noise (about 0.9 e−/pixel, Grogin et al., 2011), σ^2_{amb} is the total ambient variance in the hot column, and n is the number of raw images combined to create the superbias. The factor of 9/8 accounts for the added noise from the eight neighboring columns used to subtract off the local background.

Next, we determine which columns contain hot sections that are well-detected. The standard error on the mean excess corresponding to the maximum S/N for each column is

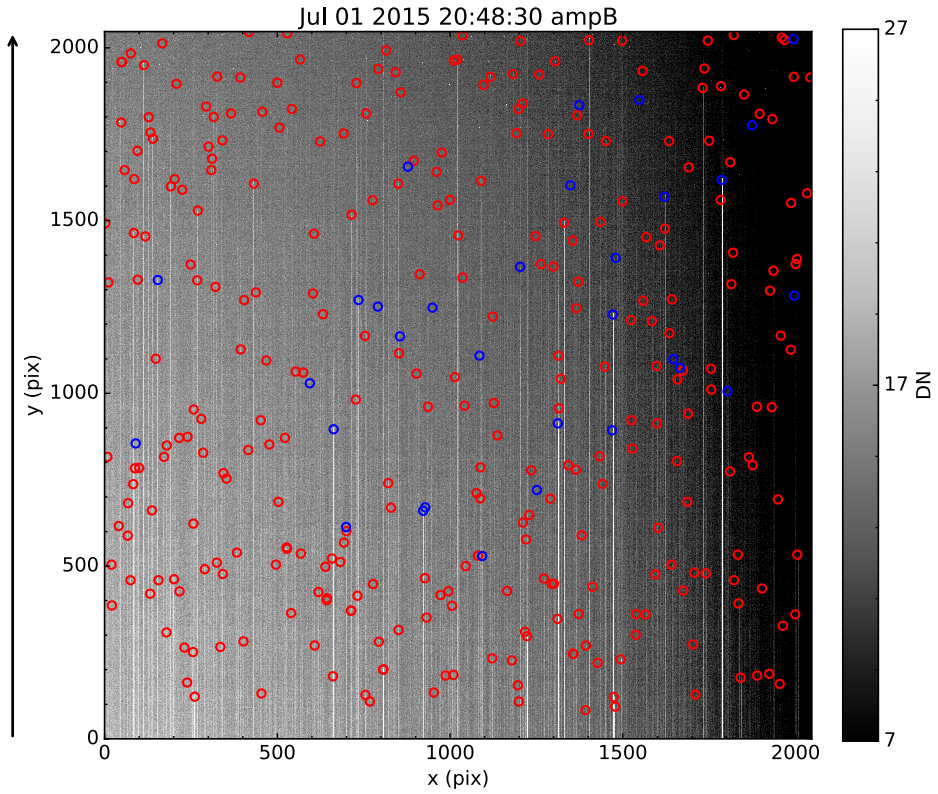

Figure 8: Top right quadrant (amp B) of the superbias from the 2015-07-01 anneal cycle. Hot columns are clearly visible as bright columns extending upward from the bottom of the frame. The circles mark the starting point of each hot column, with the red and blue circles representing stable and unstable columns, respectively, as discussed in Section 3.3. The black arrow on the left side represents the readout direction.

$\sigma_{\langle a \rangle}/\sqrt{L}$. In Figure 7, we plot the fractional error of the mean excess (standard error divided by mean excess) for each column in the 2015-07-01 superbias as a function of S/N (left panel) and mean excess (right panel). We find that a fractional error of <10% corresponds to $S/N \gtrsim 10$ for the majority of columns. A mean excess >1 e− also generally equates to fractional errors <10%. In a few early superbiases, we found that some hot columns >1 e− have fractional errors up to 75 or 100%. Combining two thresholds, mean excess >1 e−, and $S/N > 10$ (gray points in right panel of Figure 7), allows us to identify well-detected columns in all superbiases tested.

In Figure 8, we show the top right quadrant (amp B) of the superbias from the 2015-07-01 anneal cycle with circles marking the locations of the starting point of each hot column we detect with this method. The red and blue circles mark stable and unstable hot columns, respectively, as determined by the analysis discussed in Section 3.3.

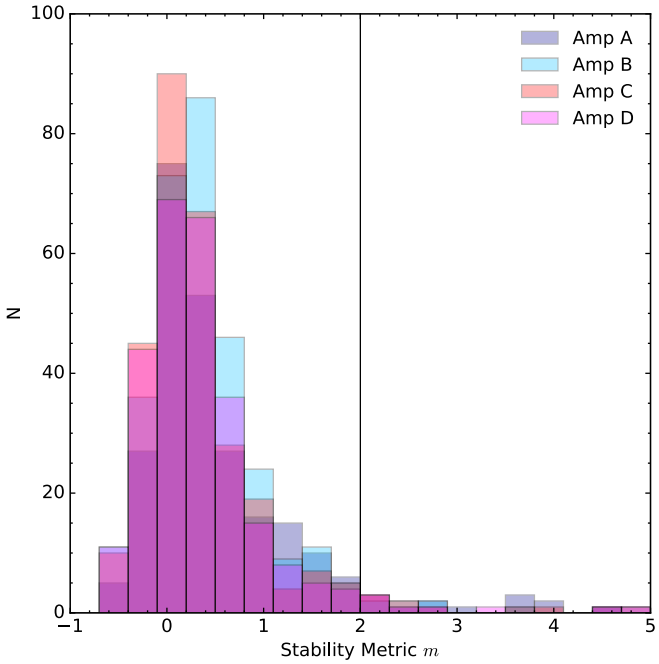

Figure 9: Distributions of stability metric m for hot columns selected from the 2015-07-01 superbias. Each quadrant's histogram is color-coded. The vertical black line represents the threshold in stability metric that we use to differentiate between stable ($m < 2$) and unstable ($m > 2$) hot columns.

3.3 Determine Stability of Hot Columns

For each of the well-detected hot columns identified by the method in Section 3.2, we determine if the excess signal is stable over the time period spanned by the raw biases. If it is stable, the hot column will be included in the superbias ERR extension, whereas if it is unstable, the hot column will be flagged in the superbias DQ extension. We define the stability metric m, as

$$m = \frac{\sigma_{\rm obs}^2 - \sigma_{\rm exp}^2}{\sigma_{\rm exp}^2}, \tag{2}$$

where $\sigma_{\rm obs}$ and $\sigma_{\rm exp}$ are the observed and expected noise, respectively, in the mean excess values. If the column varies as expected, m should be zero.

We use the set of raw bias images listed in the header HISTORY keyword of the superbias to calculate the stability metric for each column. To measure $\sigma_{\rm obs}$, we find the mean excess of the column in each individual bias (using the same background-removal method as in Section 3.2), multiply by the length of the column to get the total signal, and take the standard deviation. The expected noise is

$$\sigma_{\rm exp} = \sqrt{\langle\langle a \rangle\rangle\, L + 9/8(\mathrm{RN}^2 L + \mathrm{B}^2 L + \sigma_{\rm amb}^2)} \tag{3}$$

where $\langle\langle a \rangle\rangle$ is the mean of all of the mean excess values from the bias frames, and the other

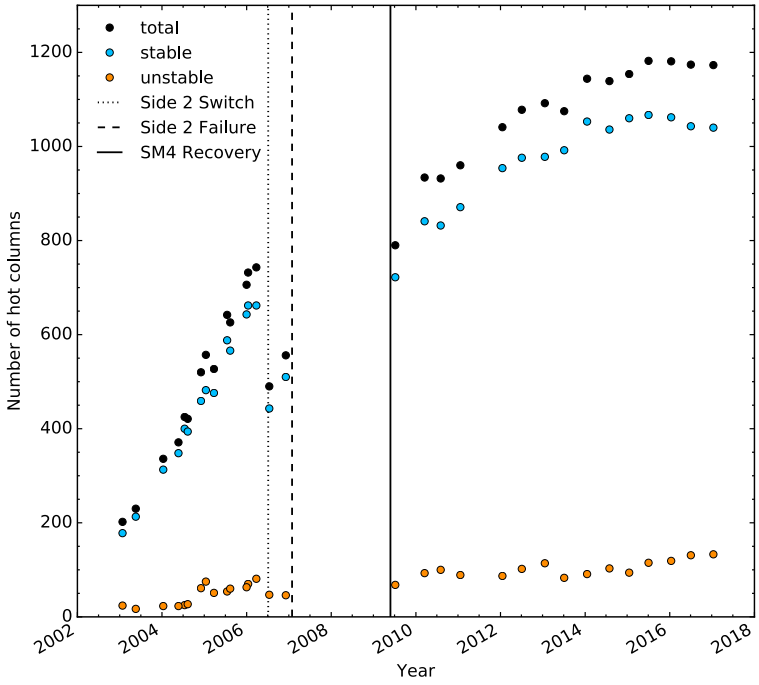

Figure 10: Number of hot columns identified in superbiases using the methods described in Sections 3.2 and 3.3 as a function of time since ACS was installed. The black, blue, and orange points are the total, number of stable, and number of unstable hot columns, respectively. The dates of the switch to side 2 electronics, the failure of side 2 electronics, and the SM4 recovery of ACS/WFC are also indicated by the dotted, dashed, and solid black lines, respectively.

variables are as defined in Eq. 1.

In Figure 9, we plot the distribution of measured stability metrics for hot columns in bias frames from the 2015-07-01 superbias. The medians of the distributions of m are $\sim$0.3 for this anneal, and have increased over the history of ACS from about -0.2 to 0.4. Therefore, it appears that the mean excess values of the hot columns are generally becoming more variable as time goes on. Initally, the hot columns were largely as stable as expected, or even less so, and now they vary a bit more than expected. Further analysis is necessary to understand why this is the case. For this work, we select a threshold of $m < 2$ to designate a hot column as stable. This threshold value corresponds to a 4 to 5 NMAD positive deviation from the median of the distribution for recent anneal cycles.

In Figure 10, we plot the total number of hot columns identified in a sample of superbiases from the lifetime of ACS. We also show how many are stable and unstable. The overall trend is reminiscent of the trends in Figures 1 through 4, with a dramatic increase in the number of hot columns before the switch to side 2 electronics and a more gradual increase post-SM4. The overall proportion of stable to unstable hot columns has remained fairly constant with time, $\sim$90% stable and $\sim$10% unstable.

3.4 Update ERR and DQ Extensions

Once we have determined which hot columns are stable and unstable, we can construct new ERR and DQ extensions for the superbias. For the ERR extension, we first generate an array for each quadrant to contain the variance contribution, in $(e-)^2$, of the stable hot columns. At the location of each stable hot column, we populate the pixels with the column's mean excess value as calculated in Section 3.2, which is approximately equal to the variance, as shown in Section 2.2. We then concatenate the arrays for all four quadrants into the proper orientation for the ACS/WFC detector and add rows and columns of zeros to represent the physical prescan and virtual overscan.

Next, we add the ambient variance arrays, generated as described in Section 3.1, to the stable hot column variance arrays, and take the square root of the result to obtain units of electrons. These are the final error arrays that represent the readout dark contribution to the error budget of every full-frame ACS/WFC image. To create the final ERR extension for the superbias, we convert the existing ERR extension of the superbias to units of electrons, add it in quadrature with the final readout dark error arrays, and convert the result back to units of DN. In Figure 11, we show the final ERR extension for the 2015-07-01 superbias. The ambient variance increase gradients are clearly visible, and increase linearly away from the amplifiers. Many of the stable hot columns are also visible, extending upward and downward from the center line[6].

Finally, we create a new DQ extension for the superbias. We generate an array of zeros for each quadrant, and populate the locations of each unstable hot column as determined in Section 3.3 with the data quality flag representing bias structure, 128. We concatenate the arrays for all four quadrants into the proper orientation for ACS/WFC and add rows and columns of zeros for the physical prescan and virtual overscan. The existing superbias DQ extension is not combined with the new DQ extension, it is simply replaced.

4 Conclusions

In this report, we have shown that the excess dark current accumulated during readout of the ACS/WFC detectors is significant, and in general has been increasing since ACS was installed on HST, likely due to radiation damage. The readout dark signal is removed from the SCI extensions of all science data during the bias correction step in CALACS. However, additional noise from readout dark is not currently taken into account. The purpose of this report is to measure the additional noise due to readout dark, determine the stability of hot columns that arise during readout, and account for these effects in the ERR and DQ extensions of each superbias.

We followed up on the previous study of ACS/WFC readout dark presented in CG14. We find that the simulated readout dark variance increase in ambient pixels is substantially less than measured in observed data. In addition, we find that the readout dark signal accrued in simulated hot columns generally does not agree with the excess variance in observed hot columns, especially for the hottest columns. We therefore turn to estimating the noise

[6]Not all stable hot columns are visible in order to ensure the figure is of reasonable resolution and file size.

contribution of the readout dark effects directly from bias images.

In our analysis, we find that the increase in variance across each ACS/WFC detector chip due to ambient readout dark noise is currently $\sim$5.2 (e$-$)^2. We identify hot columns from the superbias image that are at least 1 e$-$ brighter than their neighbors and have a S/N of at least 10. The stability of each hot column is determined by comparing the observed variance in the hot column's excess with its expected variance given Poisson statistics. We choose a threshold value in our stability metric that designates 90% of hot columns as stable and 10% as unstable in recent anneal cycles. Using these criteria, we add the additional ambient gradient in readout dark noise in quadrature with the stable hot column noise, and combine the result with the existing superbias ERR extension. We also flag the unstable hot columns with the bias structure flag, 128, in the superbias DQ extension. A new version of the ACS reference file pipeline will implement these changes to the superbias creation procedure, and new superbiases will be delivered in the near future.

Acknowledgements

The authors would like to thank the following ACS team members for their useful comments: Ralph Bohlin, Nimish Hathi, Roberto Avila, Samantha Hoffmann, Marco Chiaberge, Tyler Desjardins, and Nate Miles.

References

Borncamp, D., Grogin, N., Bourque, M., & Ogaz, S. 2017, Pixel History for Advanced Camera for Surveys Wide Field Channel, ACS ISR 2017-05, STScI

Coe, D., & Grogin, N. 2014, Readout Dark: Dark Current Accumulation During ACS/WFC Readout, ACS ISR 2014-02, STScI

Golimowski, D., Cheng, E., Loose, M., et al. 2011, ACS after Servicing Mission 4: The WFC Optimization Campaign, ACS ISR 2011-04, STScI

Grogin, N. A., Lim, P.-L., Maybhate, A., Hook, R. N., & Loose, M. 2011, Post-SM4 ACS/WFC Bias Striping: Characterization and Mitigation, ACS ISR 2011-07, STScI

Lim, P.-L., Ogaz, S., Armstrong, A., et al. 2012, Bias and Dark Calibration of ACS/WFC Data: Post-SM4 Automated Pipeline, ACS TIR 2012-01, STScI

Lucas, R. A., & et al. 2016, ACS Data Handbook, Version 8.0 (Baltimore: STScI)

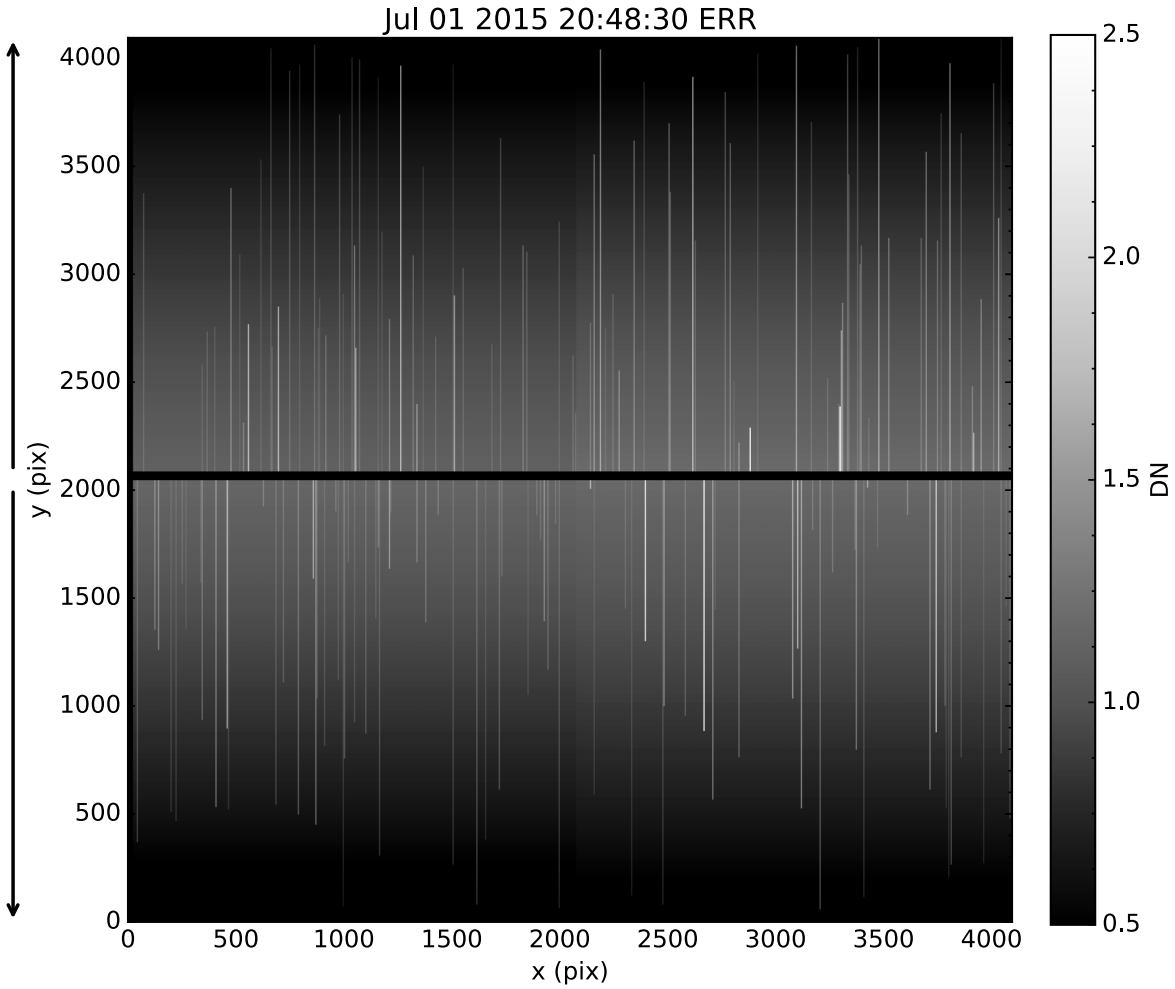

Figure 11: ERR extension, including contribution from the readout dark, of the superbias from the 2015-07-01 anneal cycle in units of DN. Both the ambient contribution to the noise and stable hot columns are clearly visible. The black arrows represent the readout directions for each chip.